



HAL
open science

Magnetodielectric Material for VHF Antenna Devices Tunable by a Low DC Magnetic Field

Alexis Chevalier, Hanadi Breiss, Antoine Hoz, Jean-Luc Mattei

► **To cite this version:**

Alexis Chevalier, Hanadi Breiss, Antoine Hoz, Jean-Luc Mattei. Magnetodielectric Material for VHF Antenna Devices Tunable by a Low DC Magnetic Field. IEEE Transactions on Magnetics, inPress, pp.1-5. 10.1109/TMAG.2023.3281491 . hal-04152085

HAL Id: hal-04152085

<https://hal.univ-brest.fr/hal-04152085>

Submitted on 5 Jul 2023

HAL is a multi-disciplinary open access archive for the deposit and dissemination of scientific research documents, whether they are published or not. The documents may come from teaching and research institutions in France or abroad, or from public or private research centers.

L'archive ouverte pluridisciplinaire **HAL**, est destinée au dépôt et à la diffusion de documents scientifiques de niveau recherche, publiés ou non, émanant des établissements d'enseignement et de recherche français ou étrangers, des laboratoires publics ou privés.

Magnetodielectric Material for VHF Antenna Devices Tunable by a Low DC Magnetic Field

Alexis Chevalier¹, Hanadi Breiss¹, Antoine Hozz¹ and Jean-Luc Mattei¹

¹ Lab-STICC, UMR 6285, Université de Bretagne Occidentale, F-29238 Brest, France

This study presents the performance of a magneto-dielectric material (MDM) specially developed to enable the tunability of antenna devices operating in the VHF band. A current flowing through the sample, which creates a DC magnetic field inside the sample with the same symmetry as the magnetic domains, controls the magnetic susceptibility variation of the MDM. By changing the magnetization state of the MDM with a low DC magnetic field of 740 A.m⁻¹, a tunability of 40% can be observed. The MDM tunability at VHF frequencies is also highlighted by microwave measurements for different magnetization states.

Index Terms— ferrimagnetic materials, magnetic susceptibility, magnetization state, tunable VHF device.

I. INTRODUCTION

Reducing the size of antennas for the VHF band (30 MHz–300 MHz) is an important issue for the airborne systems industry as it can reduce the weight of aircraft and improve their aerodynamic shape. Nevertheless, antenna integration for the VHF band is critical since the wavelengths are large at those frequencies and will lead to reduced antenna performances following the fundamental laws [1]. Magneto-dielectric materials (MDM) with a relative permittivity $\epsilon_r > 1$ and relative permeability $\mu_r > 1$ have been used in the last few years as a promising solution for antenna miniaturization and tunability. Indeed, MDM have a high refractive index $\sqrt{\epsilon_r \mu_r}$, suitable for antenna miniaturization, and allow better performance than high permittivity dielectric substrates whose drawbacks are a narrow bandwidth and low efficiency [2]–[5]. A typical efficient strategy to miniaturize an inverted F-antenna loaded with magneto-dielectric material is proposed in [6]. The problem of the tunability of antenna devices controlled by the application of a continuous magnetic field is complicated by the value of the field strength required ($>32 \text{ kA.m}^{-1}$) for their implementation, due to the importance of the shape demagnetizing effect [7]. To overcome this effect, we chose to use MDM that are toroidal in shape, with the magnetic domain walls adopting an approximately orthoradial symmetry. The permeability could then be easily modified by a magnetic field of the same symmetry, without the appearance of demagnetizing shape effects. Our main objective was to vary the magnetic susceptibility value of such a tunable MDM using a DC magnetic field lower than 800 A.m^{-1} , with the aim of achieving a tunable antenna by currents lower than 10 A.

II. SAMPLE PREPARATION AND CHARACTERIZATION

A polycrystalline NiZnCoCu ferrite especially prepared by Lab-STICC was used. It was obtained from powders synthesized by co-precipitation [4]. Nanoparticles composed of $\text{Ni}_x\text{Zn}_y\text{Cu}_z\text{Co}_{1-x-y-z}\text{Fe}_{1.98}\text{O}_4$ ferrites were prepared by a co-precipitation method using high purity nickel chloride hexahydrate, zinc chloride, cobalt chloride hexahydrate, iron (III) chloride hexahydrate (all 99.9%, Aldrich), copper (II) chloride dihydrate (99%, Aldrich), and sodium hydroxide

(99.9%, Merck). The precise composition is not specified for confidentiality reasons. These starting materials were used to make 1M solutions with deionized and double distilled water. Then, a part of sodium hydroxide was taken from approximately 1800 ml 1M NaOH in deionized and double distilled water, which was heated to boiling. Nickel chloride, cobalt chloride, zinc chloride, copper chloride, and iron III chloride solutions with appropriate proportions were poured into the boiling solution of NaOH under vigorous stirring. Mixing made it possible to avoid undesired segregation of phases. The reaction was allowed to continue for 30 min–40 min at temperatures of 80°C – 100°C under vigorous stirring. After the reaction, the vessel was cooled to ambient temperature to allow the particles to precipitate. The suspension was washed several times with deionized and distilled water until its pH value reached 8. The suspension was then dried in an electric oven, and crushed. The powders obtained were pressed either into cylindrical pellets for physicochemical analysis or into toroidal shapes for microwave measurement at a pressure of 32 MPa using a uniaxial hydraulic press. Shrinkage measurements were taken on the pellet sample with a Netzsch DIL402 dilatometer during heating from room temperature to 1000°C at a heating rate of 3.5 K/min (Fig. 1).

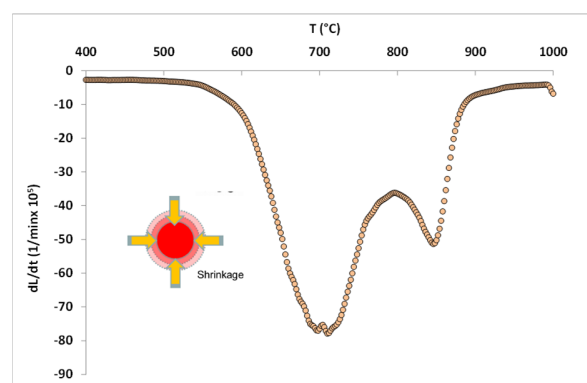


Fig. 1. Relative speed of shrinkage (dL/dt) showing two maximum peaks.

Results demonstrate that the stoichiometric composition of $\text{Ni}_x\text{Zn}_y\text{Cu}_z\text{Co}_{1-x-y-z}\text{Fe}_{1.98}\text{O}_4$ has two maximum shrinkage peaks, occurring at $T = 700^\circ\text{C}$ and at $T = 848^\circ\text{C}$. The first maximum

can be identified as a calcining process, which usually occurs at 900°C–1000°C for micrometric ferrite grains [8], but at lower temperature for nanometric grains because the fine powders prepared by chemical methods have higher reactivity [9]. Moreover, CuO addition is known to lower sintering process temperatures [8]. This process is a solid-state chemical reaction that helps homogenize the material. It consists of the interdiffusion of oxides into a chemically and crystallographically uniform structure. The second maximum ($T = 848^\circ\text{C}$) corresponds to the sintering stage. The sintering process serves to complete the interdiffusion of the component metal ions into the lattice to develop the microstructure (the growth of grains and way of coming together as porosity decreases) appropriate for the intended applications. It is known that densification of ferrites is achieved by grain-boundary diffusion, and that grain growth is determined by grain-boundary migration. Consequently, the toroidal sample was finally annealed in an air atmosphere at a temperature between 900°C and 950°C. The precise temperature value was chosen from the shrinkage measurements. It should be noted that there was no pre-sintering procedure for these samples. This was because the reactivity of ferrite powder was then expected to be lowered, which would contribute to maintaining moderate mean grain size during annealing, while it is established that CuO in the microstructure optimized the sintering process. The material in this formation is expected to retain a fairly high defect concentration during grain growth, which is desirable in our study. Indeed, the domain walls are expected to contribute to the permeability; however, at the same time, the mobility of the domain walls is moderated by these defects and also to the local anisotropy induced by Co^{2+} ions [10].

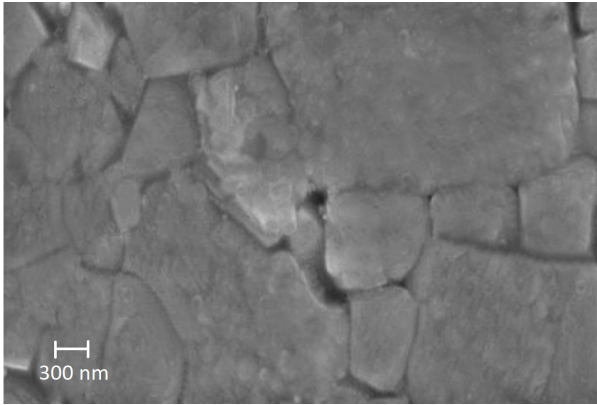


Fig. 2. SEM image of sample $\text{Ni}_x\text{Zn}_y\text{Cu}_z\text{Co}_{1-x-y-z}\text{Fe}_{1.98}\text{O}_4$ ferrite

Fig. 2 presents a Scanning Electron Microscopy image of the developed MDM. Due to partial sintering; the microstructure shows intergranular porosity and inhomogeneous grain sizes ranging from a few hundred nanometers to a few micrometers.

Fig. 3 presents the XRD patterns and Rietveld refinement analysis for the MDM sample. The experimental intensity data (black dots) matches with the calculated theoretical line profile (red line) indicating that a pure cubic spinel crystal structure with $\text{Fd}\bar{3}\text{-m}$ space group (code_ICSD 38961) was obtained for this sample. The occurrence of secondary phases or impurities

remains below the detection limit. The computed lattice parameter (a) is 8.397 Å and the crystallite size is 172 nm.

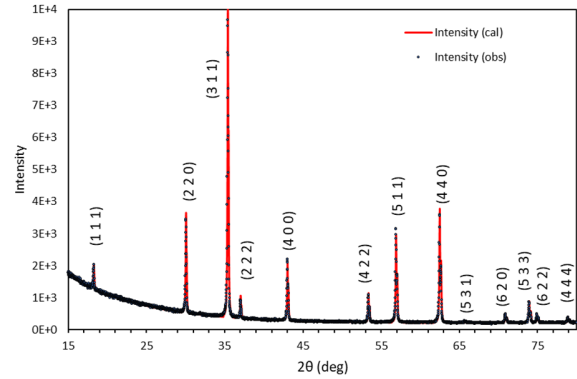


Fig. 3. XRD patterns of samples $\text{Ni}_x\text{Zn}_y\text{Cu}_z\text{Co}_{1-x-y-z}\text{Fe}_{1.98}\text{O}_4$ ferrites

III. MAGNETIC CHARACTERIZATION

Previous studies have shown that in polycrystalline materials with low anisotropy and several axes of easy magnetization, a sintering treatment at low temperature allows grains free of defects to be obtained [11], [12]. Furthermore, if the sample is toroidal in shape, the minimization of magnetostatic energy leads to a configuration of magnetic moments and domain walls along the orthoradial direction. Even though straightforward microanalysis data are not yet available, in such materials as the developed MDM sample, the domain wall motion is the main factor controlling the magnetization mechanisms. We therefore proposed to achieve initial susceptibility tunability by acting on the domain wall configuration through the application of a static magnetic field (Fig. 4b).

The initial magnetic susceptibility is measured by a laboratory-developed hysteresis meter based on the magnetic transformer method. The primary winding is connected to a low AC voltage to create a low intensity AC magnetic field h in the sample, while the secondary winding is connected to an EGG Princeton 5302 lock-in amplifier to measure the AC magnetic flux density b (Fig. 4a).

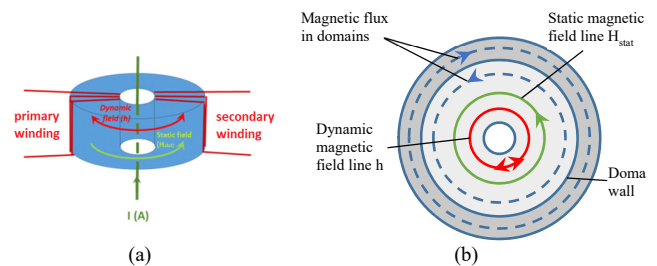


Fig. 4. Measurement setup (a) and ideal domain wall distribution (b)

The benefit of the lock-in amplifier is twofold: it makes it possible, on the one hand, to measure signals of low amplitude as is the case for initial susceptibility and, on the other hand, to directly integrate the signal in the secondary winding, giving access to the magnetic induction flow b .

The initial magnetic susceptibility is then calculated as $\chi = b/(\mu_0 h) - 1$. In addition, a single control wire running through

the toroidal sample allows a DC magnetic field H_{stat} to be superimposed on the AC magnetic field h in the same orthoradial direction (Fig. 4a). This is a key point of the experiment because it avoids the appearance of demagnetizing shape effects, the orthoradial configuration ensuring the loop back of the magnetic flux. The DC current I flowing in the control wire can be adjusted to change the magnetization state of the sample and thus modify its susceptibility. According to the characteristics of the experimental setup, the mean static field H_{stat} created in the sample is proportional to the current: $H_{\text{stat}} (\text{A}\cdot\text{m}^{-1}) = 74.1 \times I (\text{A})$.

The change in initial susceptibility is closely related to the magnetization state, which is set by the control current. Due to the orthoradial symmetry of the domain walls, magnetization mechanisms in this type of ferrimagnetic material with low magnetocrystalline anisotropy can be represented by the Globus model [13], [14], which shows that the susceptibility is linked to the grain size of the sample. In this model, the magnetic behavior of the material can be represented by that of a spherical grain divided into two magnetic domains whose Bloch wall is fixed to the grain boundary along its circumference (Fig. 5).

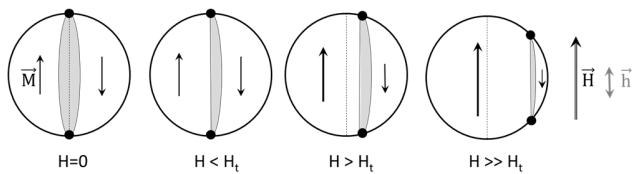


Fig. 5. Model of ideal magnetic grain divided into two magnetic domains. The wall moves under static field H and vibrates under dynamic field h . Shaded areas represent wall vibration.

The domain wall can vibrate under the action of the dynamic field h and bulge (reversible) and move (irreversible) under the action of the static field H . The domain wall moves from its central position ($H=0$) when the static field becomes greater than a threshold field H_t . The initial susceptibility of the material then becomes lower as the diameter of the domain wall decreases.

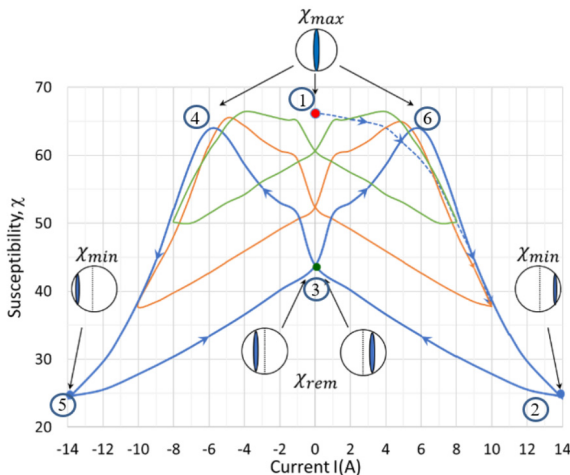


Fig. 6. Initial susceptibility measured at 10 kHz for currents up to 14 A. (In Green: $I_{\text{max}} = 8$ A, in Orange: $I_{\text{max}} = 10$ A, in blue: $I_{\text{max}} = 14$ A)

Fig. 6 shows the initial susceptibility of the developed MDM measured for a set of control currents up to 14 A. Curves obtained with I higher than 4 A show a notable variation and hysteretic behavior.

Let us describe an initial susceptibility measurement cycle, represented by points 1 to 6 in Fig. 6. In the demagnetized state (point 1), the domain wall is located in the middle of the grain; the susceptibility is equal to its maximum value $\chi_{\text{max}} = 66$. As the current increases, the susceptibility decreases first under the effect of the magnetic thrust acting on its surface, which constrains the vibration of the wall, then under the effect of the rightward displacement of the wall to a position where its diameter is smaller. The susceptibility reaches its minimum value χ_{min} (point 2) for the maximum current ($\chi_{\text{min}} = 24$ for $I_{\text{max}} = 14$ A). Then, as the current decreases, the domain wall moves back to the left to minimize the magnetostatic energy and tends to return to its initial position; the susceptibility then increases slightly. Due to pinning effects by the grain boundary, the domain wall does not return to its central position and the susceptibility takes a remanent value χ_{rem} for $I = 0$ (point 3), which depends on the maximum current reached beforehand ($\chi_{\text{rem}} = 44$ after $I_{\text{max}} = 14$ A). As the current reverses, the domain wall moves in the opposite direction and approaches the central position. The susceptibility increases until it reaches a value close to the maximum (point 4) for a central position of the domain wall, which corresponds to the demagnetized state and is obtained for a so-called coercive current. Increasing the current in the negative values, the susceptibility decreases to the same minimum value as in the first branch (point 5). Decreasing the negative current to zero, we again find the remanent susceptibility (point 3) but with a non-central wall position symmetrical to that of the first branch. Finally, by increasing the current in positive values, the domain wall moves to reach the central position (point 6); the cycle loops for a current reaching the maximum value. Note that the maximum susceptibility (points 4 or 6) decreases with the increase of the maximum current because, although the domain wall is brought back to the central position, the applied static field is not zero and a magnetic thrust acts on the wall surface limiting its vibration.

The coercive current necessary to recover the initial susceptibility value of the demagnetized state (points 4 and 6) is not constant and depends on the value of the maximum current previously reached. It becomes higher as I_{max} becomes larger. This is because we are making minor hysteresis loops and do not saturate the sample with the static current available with this experimental setup.

Fig. 7 shows hysteresis loops measured in alternating field on the same measurement setup. There is no static current I in the control wire. Measurements were performed with dynamic current strengths in the primary winding, creating magnetic fields of amplitudes similar to those obtained with static currents. In the case of a maximum current $I_{\text{max}} = 10$ A, corresponding to a static field $H_{\text{stat}} = 741 \text{ A}\cdot\text{m}^{-1}$, the coercive current measured on Fig. 6 is 5 A, i.e., a field of $371 \text{ A}\cdot\text{m}^{-1}$.

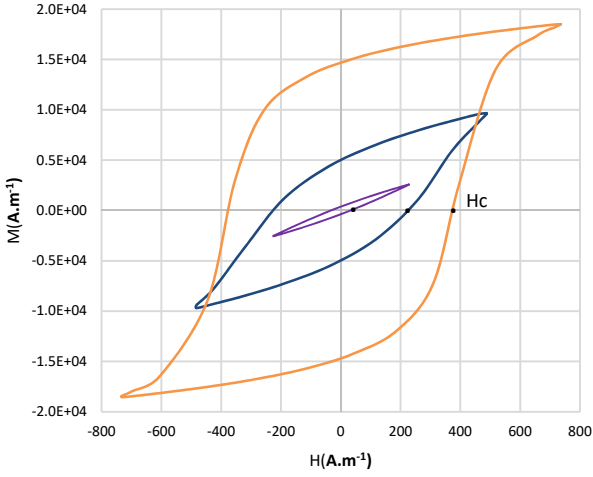


Fig. 7. Hysteresis loop measured at 10 kHz. For each loop, the coercive field H_c corresponds to $M=0$.

The hysteresis loop measured in an alternating field of the same intensity (orange curve in Fig. 6 and Fig. 7) shows a coercive field of 377 A.m^{-1} . This perfect agreement clearly shows that the initial susceptibility is governed by the wall position in the grain. Table 1 summarizes the coercive field values resulting from the hysteresis cycles $H_{c_{\text{cycle}}}$ and those measured on the initial susceptibility curves $H_{c_{\text{suscept}}}$ for several maximum field values.

TABLE I. COMPARISON OF COERCIVE FIELDS

I_{max} (A)	H_{max} (A.m^{-1})	$H_{c_{\text{suscept}}}$ (A.m^{-1})	$H_{c_{\text{cycle}}}$ (A.m^{-1})
5	371	148	142
8	593	296	300
10	741	371	377
12	889	408	405

The agreement between the values obtained by the two methods was confirmed for all current values.

Furthermore, the hysteresis loop shows a large remanence in Fig. 7. Indeed, due to porosity and potential wells related to the presence of Cobalt, the domain walls remain trapped after magnetization and do not easily return to the initial position when the field returns to zero.

IV. TUNABILITY OF THE MAGNETODIELECTRIC MATERIAL

Fig. 8 shows the dependence of the three susceptibilities χ_{max} , χ_{min} and χ_{rem} on the static applied current deduced from the initial susceptibility curves. The deviation of the susceptibility from its maximum value becomes noticeable for currents above 4 A and increases significantly up to 14 A before showing saturation for high currents. Note that the minimum susceptibility is obtained for a permanent current in the control wire. When the current is established and then stopped, the remanent susceptibility remains. Thus, a fairly good level of tunability can be obtained with this material in the remanent state without maintaining the current. This is a very interesting

feature for embedded systems where power management is required. The tunability of the VHF device will be directly related to that of the susceptibility, which is defined by $(\chi_{\text{max}} - \chi_{\text{min}}) / \chi_{\text{max}}$.

As shown in Fig. 8, good MDM tunability can be achieved with moderate currents: up to 40% with $I = 10 \text{ A}$, to which corresponds a DC magnetic field $H_{\text{stat}} = 740 \text{ A.m}^{-1}$.

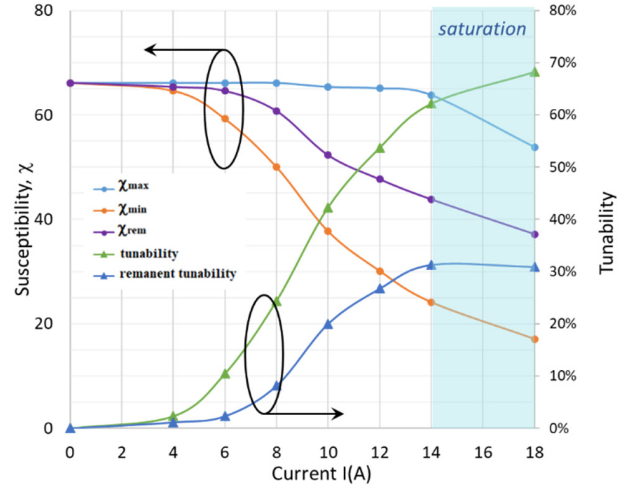


Fig. 8. Initial susceptibility and tunability measured at 10 kHz. (left scale: susceptibility; right scale: tunability).

To work with remanence and avoid maintaining a static current, a current pulse can briefly magnetize the sample. When the sample is briefly polarized (10 A) and the current is turned off, the tunability remains at 20%. Higher tunability can be achieved at higher currents e.g. 62% and 31% by maintaining the control current of 14 A or not, respectively.

V. MICROWAVE MEASUREMENTS

To verify the tunability of the material at the operating frequencies of VHF devices, microwave measurements were performed using the APC7 coaxial transmission line method [15] and Agilent 8753ES network analyzer. However, adding a DC control current in the transmission line requires the use of bias tees, which are usually limited to currents below 5 A and which, moreover, cause severe perturbations in the measured S-parameters. We therefore chose to separate the magnetization step and the microwave measurements. The sample was first polarized with the selected current on the permeameter setup, brought into its remanent state, and then measured in microwave transmission line without static current.

Fig. 9 shows the susceptibility spectra measured by the transmission line method in the 10 MHz–1 GHz frequency band for three different states of magnetization. Magnetic losses remain low in the 10 MHz–80 MHz frequency band, making these materials suitable for VHF applications. The permeability spectra show only one dispersion region, which is attributed to domain wall motion. Indeed, in coaxial geometry, the natural ferromagnetic resonance (FMR) occurs only if there is a magnetization component perpendicular to the dynamic field h , which is in the orthoradial direction.

In the developed MDM sample, we assumed that the domain walls and spins are aligned in the orthoradial direction. There is no perpendicular magnetization component and, therefore, FMR cannot be excited. Thus, the resonance observed in Fig. 9 is a wall resonance due to inhomogeneous grain size or wall discontinuity in the sample [16]-[17]. The experimental microwave data substantiate our hypothesis of a toroidal configuration of the domain walls and spins.

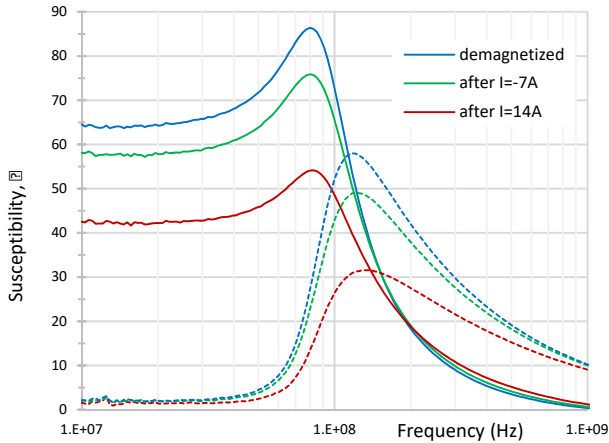


Fig. 9. Microwave susceptibility for three magnetization states. (solid lines: real part; dashed lines: imaginary part).

As shown in Fig. 9, the MDM tunability is well demonstrated: a control current of 14 A makes the susceptibility change from 65 in the demagnetized state to 43 in the remanent state, resulting in a remanent tunability of 33% very close to that measured at 10 kHz. Subsequently, an intermediate magnetization state, obtained after application of a negative current of 7 A, makes it possible to recover a susceptibility equal to 58. This clearly demonstrates the tunability of the MDM in the VHF band through the control of its magnetization state. The measurements in coaxial line also demonstrated that the permittivity of the developed material is close to 12, non-dispersive in the measured frequency band, and independent of the magnetization state.

VI. CONCLUSION

This work demonstrates the suitability of the developed MDM for use in VHF tunable devices. A tunability of the magnetic susceptibility up to 40% can be achieved for currents below 10 A, i.e., for a DC magnetic field less than $800 \text{ A}\cdot\text{m}^{-1}$. A promising result for future applications is the tunability of the MDM up to 30% that can be reached without permanently holding a current. After a short pulse, the control current can be switched off, which allows operation in the remanent state.

ACKNOWLEDGMENTS

The authors gratefully acknowledge R. Lebourgeois who provided the SEM microstructure image. This work was supported in part by the French National Research Agency under Grant ANR-21-ASTR-0020 (TOCCATA project).

REFERENCES

- [1] H. A. Wheeler, "Fundamental Limitations of Small Antennas," *Proc. IRE*, vol. 35, no. 12, pp. 1479–1484, Dec. 1947.
- [2] F. Canneva, F. Ferrero, A. Chevalier, J. Ribero, J. Mattei, P. Queffelec, and R. Staraj, "Miniature Reconfigurable Antenna with Magneto Dielectric Substrate for DVB-H Band," *Microw. Opt. Technol. Lett.*, vol. 55, no. 9, pp. 2007–2011, Sep. 2013.
- [3] J. P. Cortes Nino, P. Queffelec, A. Chevalier, G. Verissimo, and J.-L. Mattei, "Modeling antennas printed on magnetized substrate: Application to the design of a tunable PIFA antenna," in *2015 European Microwave Conference (EuMC)*, 2015, pp. 933–936.
- [4] J.-L. Mattei, E. Le Guen, and A. Chevalier, "Dense and half-dense NiZnCo ferrite ceramics: Their respective relevance for antenna downsizing, according to their dielectric and magnetic properties at microwave frequencies," *J. Appl. Phys.*, vol. 117, no. 8, p. 084904, Feb. 2015.
- [5] Q. Li, Y. Chen, C. Yu, L. Young, J. Spector, and V. G. Harris, "Emerging magnetodielectric materials for 5G communications: 18H hexaferrites," *Acta Mater.*, vol. 231, p. 117854, 2022.
- [6] L. Batel, J.-L. Mattei, V. Laur, A. Chevalier, and C. Delaveaud, "Tunable Magneto-Dielectric Material for Electrically Small and Reconfigurable Antenna Systems at Vhf Band," *Ceramics*, vol. 3, no. 3, pp. 276–286, Jul. 2020.
- [7] E. Andreou, T. Zervos, A. A. Alexandridis, and G. Fikioris, "Magnetodielectric Materials in Antenna Design: Exploring the Potentials for Reconfigurability," *IEEE Antennas Propag. Mag.*, vol. 61, no. 1, pp. 29–40, Feb. 2019.
- [8] A. Goldman, *Modern Ferrite Technology*, 2nd ed. 2006.
- [9] M. H. Weng, T. J. Liang, and C. L. Huang, "Lowering of sintering temperature and microwave dielectric properties of BaTi4O9 ceramics prepared by the polymeric precursor method," *J. Eur. Ceram. Soc.*, vol. 22, no. 9–10, pp. 1693–1698, Sep. 2002.
- [10] U. L. Ribeiro, R. S. Nasar, M. C. Nasar, and J. H. de Araújo, "Liquid phase sintering of ferrite of NiCuZn with low magnetic permeability for miniaturization," *Ceram. Int.*, vol. 44, no. 1, pp. 723–727, Jan. 2018.
- [11] A. Globus, V. Cagan, H. Pascard, M. Le Floch, and J. Loaec, "Coherence of magnetic phenomena in ferrimagnetic materials as a function of spin and domain wall topography," in *Ferrites: Proc. of the international conference*, 1980.
- [12] J. Loaec, M. Le Floch, and A. Globus, "Change of wall topography in soft Ferrites by isotropic and anisotropic external pressures," *IEEE Trans. Magn.*, vol. 15, no. 6, pp. 1861–1863, Nov. 1979.
- [13] A. Globus, P. Duplex, and M. Guyot, "Determination of initial magnetization curve from crystallites size and effective anisotropy field," *IEEE Trans. Magn.*, vol. 7, no. 3, pp. 617–622, Sep. 1971.
- [14] A. Globus, "Some physical considerations about the domain wall size theory of magnetization mechanisms," *J. Phys. Colloq.*, vol. 38, no. C1, pp. C1-1-C1-15, Apr. 1977.
- [15] J. Baker-Jarvis, M. D. Janezic, J. H. Grosvenor, and R. G. Geyer, "Transmission/reflection and short-circuit line methods for measuring permittivity and permeability," *Natl. Inst. Stand. Technol.*, vol. Tech. Note, 1993.
- [16] A. Globus and M. Guyot, "Control of the susceptibility spectrum in polycrystalline ferrite materials and frequency threshold of the losses," *IEEE Trans. Magn.*, vol. 6, no. 3, pp. 614–617, Sep. 1970.
- [17] U. Varshney and R. K. Puri, "The effect of substitutions of Sn⁴⁺ and Zn²⁺ ions on the magnetic properties of nickel ferrites," *IEEE Trans. Magn.*, vol. 25, no. 4, pp. 3109–3116, Jul. 1989.